
Enzyme adaptation to alkaline pH: Atomic resolution (1.08 Å) structure of phosphoserine aminotransferase from *Bacillus alcalophilus*

ANATOLY P. DUBNOVITSKY, EVANGELIA G. KAPETANIOU, AND ANASTASSIOS C. PAPAGEORGIOU

Turku Centre for Biotechnology, University of Turku and Åbo Akademi University, Turku 20521, Finland

(RECEIVED August 5, 2004; FINAL REVISION August 26, 2004; ACCEPTED August 26, 2004)

Abstract

The crystal structure of the vitamin B₆-dependent enzyme phosphoserine aminotransferase from the obligatory alkaliphile *Bacillus alcalophilus* has been determined at 1.08 Å resolution. The model was refined to an *R*-factor of 11.7% (*R*_{free} = 13.9%). The enzyme displays a narrow pH optimum of enzymatic activity at pH 9.0. The final structure was compared to the previously reported structure of the mesophilic phosphoserine aminotransferase from *Escherichia coli* and to that of phosphoserine aminotransferase from a facultative alkaliphile, *Bacillus circulans* subsp. *alkalophilus*. All three enzymes are homodimers with each monomer comprising a two-domain architecture. Despite the high structural similarity, the alkaliphilic representatives possess a set of distinctive structural features. Two residues directly interacting with pyridoxal-5'-phosphate are replaced, and an additional hydrogen bond to the O3' atom of the cofactor is present in alkaliphilic phosphoserine aminotransferases. The number of hydrogen bonds and hydrophobic interactions at the dimer interface is increased. Hydrophobic interactions between the two domains in the monomers are enhanced. Moreover, the number of negatively charged amino acid residues increases on the solvent-accessible molecular surface and fewer hydrophobic residues are exposed to the solvent. Further, the total amount of ion pairs and ion networks is significantly reduced in the *Bacillus* enzymes, while the total number of hydrogen bonds is increased. The mesophilic enzyme from *Escherichia coli* contains two additional β-strands in a surface loop with a third β-strand being shorter in the structure. The identified structural features are proposed to be possible factors implicated in the alkaline adaptation of phosphoserine aminotransferase.

Keywords: pyridoxal-5'-phosphate; alkaliphilicity; phosphoserine; Schiff base; protein stability; X-ray crystallography

Phosphoserine aminotransferase (PSAT; EC 2.6.1.52) catalyzes the reversible conversion of 3-phosphohydroxypyruvate to L-phosphoserine. This reaction is the second step of the major pathway of L-serine biosynthesis in many organisms, from bacterial cells to mammals including humans

(Basurko et al. 1999; Hester et al. 1999; Baek et al. 2003; de Koning et al. 2003). Except for its role in protein synthesis, L-serine serves as a source of one-carbon units and is involved in a number of important metabolic pathways (Ichihara and Greenberg 1957; Walsh and Sallach 1966; Snell 1986; de Koning et al. 2003). PSAT is a vitamin B₆-dependent enzyme, which belongs to the α family of pyridoxal-5'-phosphate (PLP) enzymes (Alexander et al. 1994). PSAT is also classified as a member of the aspartate aminotransferase family of PLP enzymes (Jansonius 1998). According to the structural classification of PLP-dependent enzymes (Grishin et al. 1995), PSAT belongs to the fold type I, where it is allocated to a separated subclass (Schneider et al. 2000).

Reprint requests to: Anastassios C. Papageorgiou, Turku Centre for Biotechnology, Biocity, 5th Floor, Tykistökatu 6, Turku 20521, Finland; e-mail: apapageo@btk.utu.fi; fax: +358-2-333-8000.

Abbreviations: BALC, *Bacillus alcalophilus*; BCIR, *Bacillus circulans* subsp. *alkalophilus*; ECOLI, *Escherichia coli*; PLP, pyridoxal-5'-phosphate; PSAT, phosphoserine aminotransferase; PPIS, Protein-Protein Interaction Server; RMSD, root-mean-square deviation.

Article and publication are at <http://www.proteinscience.org/cgi/doi/10.1110/ps.041029805>.

Extremophilic microorganisms offer an attractive opportunity for investigating adaptation mechanisms in extreme environmental conditions. Proteins directly exposed to hostile environments accumulate certain structural features making them stable and active under harsh conditions. A number of studies on proteins from thermophiles, psychrophiles, and halophiles have provided some insights into the mechanisms and principles of protein adaptation to extreme temperatures and salinity (Jaenicke and Böhm 1998). However, little is known about adaptation of proteins to pH extremes. Structural studies of acidophilic xylanases from *Aspergillus kawachii* (Fushinobu et al. 1998) and *Streptomyces* sp. S38 (de Lemos Esteves et al. 2004), and maltose-binding protein from *Alicyclobacillus acidocaldarius* (Schäfer et al. 2004) have revealed some features related to the acidic stability in these protein families. Despite that various crystal structures of alkaline proteases have been reported to date, structural adaptation of these enzymes to alkaline pH has not been systematically studied. More detailed analysis of alkaline adaptation has been done by Shirai et al. in crystallographic studies of M-protease (1997) and alkaline cellulase K (2001).

The crystal structure of PSAT from *Escherichia coli* (ECOLI PSAT) has been previously reported at 2.3 Å resolution (Hester et al. 1999). Similar to other aminotransferases, ECOLI PSAT is a homodimer. Two active sites in a PSAT dimer are situated at the interface between the two monomers. The enzyme from *E. coli* shows a broad pH-optimum between pH 7.5 and pH 8.5 (Kallen et al. 1987). Using molecular replacement and ECOLI PSAT as a search model, we recently determined the crystal structure of PSAT from a facultative alkaliphile, *Bacillus circulans* subsp. *alkalophilus* (BCIR PSAT), at 1.5 Å resolution (PDB entry 1W3U; E.G. Kapetaniou, A.P. Dubnovitsky, and A.C. Papageorgiou, unpubl.). As a next step, we initiated a crystallographic study of PSAT from an obligatory alkaliphile, *Bacillus alcalophilus* (BALC PSAT) (Dubnovitsky et al. 2003). Although PSAT is a cytoplasmic enzyme (Snell 1986), the pH-optima of enzymatic activity for both BCIR PSAT and BALC PSAT are shifted toward alkaline pH in comparison to ECOLI PSAT (see Results and Discussion). Thus, comparative analysis of these enzymes may reveal structural features correlated to the elevated activity at alkaline pH.

Here, we report the crystal structure of PSAT from *B. alcalophilus* at 1.08 Å resolution. Detailed comparison of this structure to the structures of *E. coli* PSAT and *B. circulans* PSAT was carried out to provide insights into mechanisms of enzyme adaptation to alkaline conditions.

Results and Discussion

pH optimum

The enzymatic activity of BALC PSAT in the reaction of phosphoserine synthesis was measured at pH values be-

tween 7.0 and 10.0. The pH of the reaction mixture was routinely measured following the activity assay, as a significant shift in pH (0.2–0.3 units) was obtained after addition of highly acidic solution of 3-phosphohydroxypyruvate. A narrow pH optimum at pH 9.0 was found for BALC PSAT (Fig. 1). At pH 9.5, the enzyme retains more than 60% of its maximum activity, while its relative activity at pH 7.0 is less than 10%. The alkaliphilic *Bacillus* species growing at alkaline pH have been shown to maintain their cytoplasmic pH about two units less than the environmental pH (Krulwich et al. 1997). *B. alcalophilus* displays an optimum growth at pH 10.6. The cytoplasmic pH in such conditions is close to 9.0 (Horikoshi 1999), which is in good agreement with the obtained pH optimum of BALC PSAT.

Quality of the structure

The crystal structure of BALC PSAT has been determined at 1.08 Å resolution and refined to a crystallographic R -factor (R_{cryst}) of 11.7% [11.0% for $F > 4\sigma(F)$] and an R_{free} of 13.9% [13.0% for $F > 4\sigma(F)$]. To the best of our knowledge, this is the highest resolution for any PLP-dependent enzyme. Optimization of crystallization conditions by addition of glycerol, as described in Materials and Methods, improved crystals quality and allowed a complete crystallographic data collection to 1.08 Å resolution from a single crystal. The structure was refined with anisotropic B -factors for all nonhydrogen atoms and addition of hydrogen atoms at riding positions. The final model of PSAT is a homodimer, which contains two subunits and includes 5824 protein atoms, 949 water molecules with full occupancy, 30 cofactor atoms, 8 ions, and 58 atoms of different ligands (Table 1). Examination of the Ramachandran plot with PROCHECK (Laskowski et al. 1993) shows 91.9% of all nonglycine and nonproline residues in the most favored regions and 8.1% in generously allowed regions. All geometric parameters of the model, analyzed by PROCHECK, are similar to those of other structures determined at atomic

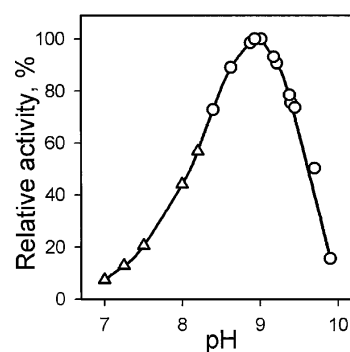


Figure 1. The pH-dependence of BALC PSAT enzymatic activity. The value of V_{max} for the reaction of phosphoserine synthesis was measured at different pH in 0.1 M HEPES (triangles) or CHES (circles).

Table 1. Crystallographic data and refinement statistics

Data set	Data set I	Data set II	
A. Data collection			
Wavelength (Å)	0.811	0.901	
Cell dimensions (Å)	143.7 × 84.3 × 67.4	144.5 × 84.8 × 67.5	
Resolution range (Å)	20–1.4 (1.44–1.40)	20–1.08 (1.11–1.08)	
Wilson <i>B</i> -factor (Å ²)	14.5	9.7	
Number of measured reflections	2,316,323	8,312,749	
Number of unique reflections	156,742	351,228	
Completeness (%)	95.6 (90.1)	99.8 (100.0)	
<i>R</i> -merge (%)	5.4 (19.7)	5.4 (37.0)	
<i>I</i> / σ (<i>I</i>)	18.1 (7.8)	32.9 (2.8)	
B. Refinement			
Resolution range (Å)		20–1.08	
Number of reflections		333,406 + 17,505	
<i>R</i> _{cryst} (%) (<i>F</i> > 0 σ)		11.7	
<i>R</i> _{free} (%) (5% of data)		13.9	
Number of observations per parameter		5.65	
Model content			
Protein residues		717	
Cofactor molecules		2	
Water molecules with full occupancy		949	
PEG molecules		4	
HEPES molecules		1	
Glycerol molecules		1	
Mg ²⁺ ions		4	
Cl ⁻ ions		4	
Deviations from ideal geometry			
Bond distances (Å)		RMSD	target σ
Angle distances (Å)		0.016	0.020
Chiral volumes (Å ³)		0.033	0.040
C sp ³		0.085	0.100
C sp ²		0.096	0.100
Anisotropic displacement parameters			
DELU (Å ²)		RMSD	target σ
SIMU (Å ²)		0.006	0.010
ISOR (Å ²)		0.056	0.040
ISOR (Å ²)		0.103	0.100
Mean isotropic equivalent <i>B</i>-factor (Å²)			
Main-chain atoms		12.9	
Side-chain atoms		18.2	
Cofactor atoms		10.8	
Water molecules		28.8	
Ramachandran plot (%)			
Residues in most favored regions		91.9	
Residues in additional allowed regions		8.1	

Values in parentheses correspond to the highest resolution shell.

resolution (Longhi et al. 1998). The root-mean-square deviations (RMSD) from ideal geometry for bond lengths, angles, chiral volumes, and deviations from target values for restraints applied to anisotropic displacement parameters calculated with SHELX-97 (Sheldrick and Schneider 1997) are summarized in Table 1. All protein atoms were included in the calculation of RMSD despite that N-terminal residues and some loops were found highly flexible in the final structure. The coordinate error assessed by a Luzzati plot is 0.05 Å.

Refinement of BALC PSAT at 1.08 Å resolution resulted in an electron density map of excellent quality for most of

the residues. However, N-terminal residues 1–3 and surface loop 210–219 in each monomer are highly disordered. In the final map, weak electron density was obtained for a number of highly mobile side chains on the solvent exposed molecular surface. Residues 215, 216, 218, and 219 (subunit A) and residue 218 (subunit B) were modeled as alanines due to incomplete electron density for the side chains. Residues 214–216 from subunit B were not modeled due to lack of sufficient density and, hence, not included in the refinement. Subunit A will be used throughout the discussion except where noted otherwise. Residues from subunit B will be marked in the text with an asterisk.

Overall structure

The overall architecture of BALC PSAT (Fig. 2) is similar to that of ECOLI PSAT (PDB entry 1BJN; Hester et al. 1999). The RMSD is 1.1 Å for 344 C $^{\alpha}$ atoms in monomer A. The main structural features of PSAT are similar to those of the other family members. Each PSAT monomer consists of a small and a large domain. Residues 16–266 form the large domain, while residues 267–360 together with N-terminal residues 1–15 belong to the small domain. The large domain contains a seven-stranded mainly parallel β -sheet with $\beta 2^{\uparrow}$, $\beta 10^{\downarrow}$, $\beta 9^{\uparrow}$, $\beta 8^{\uparrow}$, $\beta 5^{\uparrow}$, $\beta 3^{\uparrow}$, $\beta 4^{\uparrow}$ order of the strands, where only $\beta 10$ is antiparallel to the others (Fig. 2). The loop connecting strands $\beta 9$ and $\beta 10$ harbors the active site residue Lys196. Toward the dimer interface, the β -sheet is flanked by helices $\alpha 3$, $\alpha 4$, $\alpha 5$, and $\alpha 6$. Its exterior side is shielded from the solvent by helices $\alpha 1$, $\alpha 2$, $\alpha 7$, and two small strands, $\beta 6$ and $\beta 7$, which are packed close to the domains interface. At the end of helix $\alpha 7$ the polypeptide chain forms a 90° kink followed by helix $\alpha 8$ (residues 259–281), which contains the boundary between the two domains at Asp267. A large part of helix $\alpha 8$ (residues 267–281), helices $\alpha 9$ and $\alpha 10$ and five β -strands organized into two β -sheets form the small domain. One antiparallel β -sheet consists of strands $\beta 11^{\uparrow}$, $\beta 12^{\downarrow}$, and $\beta 14^{\uparrow}$. It is packed against helices $\alpha 8$ and $\alpha 10$ on one side and the large domain on the other. The second β -sheet containing small parallel strands $\beta 1$ and $\beta 13$ is bundled to helices $\alpha 9$ and $\alpha 10$. A total of six 3_{10} helices were found per monomer, but only one of them belongs to the small domain.

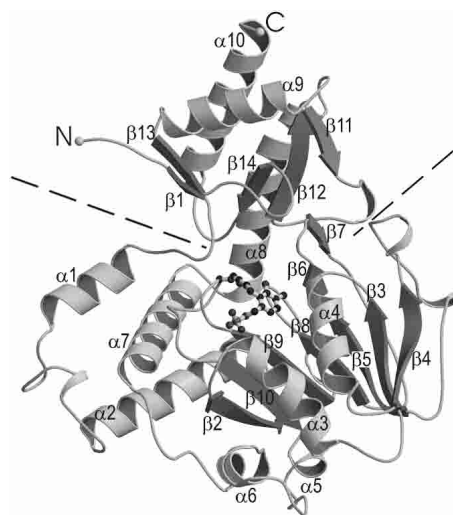


Figure 2. Ribbon diagram of the BALC PSAT monomer. The α -helices are shown in light gray and the β -strands in dark gray. Secondary structure elements and N and C termini are labeled. The dashed line depicts the boundary between the small and the large domain. The side chain of the active site residue Lys196 and the PLP molecule are shown in ball-and-stick representation. The figure was produced using MOLSCRIPT (Kraulis 1991) and Raster3D (Merritt and Murphy 1994).

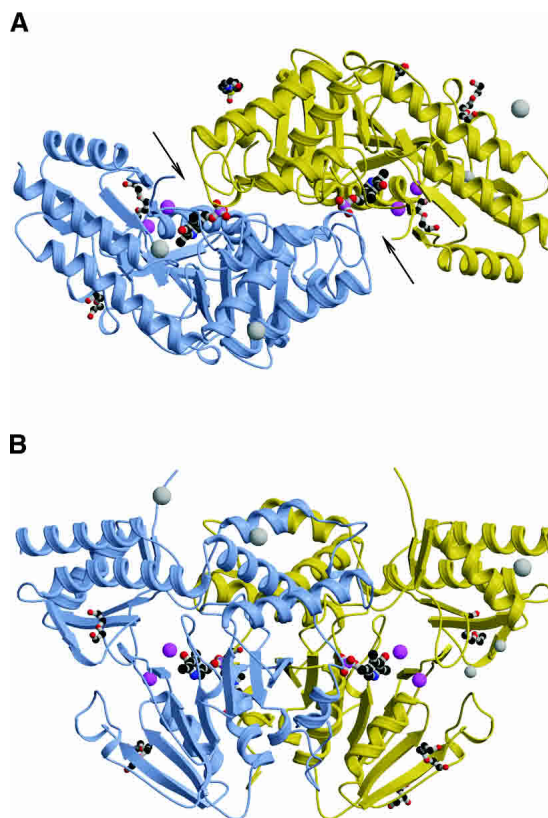


Figure 3. Ribbon representation of the BALC PSAT dimer. The two monomers are depicted in yellow and in blue, respectively. Ligands included in the final model (PLP, PEG, HEPES, glycerol) are shown in ball-and-sticks. Mg $^{2+}$ ions are shown as gray spheres and Cl $^{-}$ ions as pink spheres. (A) View along the twofold noncrystallographic axis. The active site clefts are shown with arrows. (B) BALC PSAT dimer after 90° rotation. The twofold axis in this orientation is vertical and lying within the plane of the figure. The figure was produced using MOLSCRIPT (Kraulis 1991) and Raster3D (Merritt and Murphy 1994).

PSAT dimer

Previous studies have shown that BALC PSAT is present in solution as a dimer (Dubnovitsky et al. 2003). One homodimer was found in the asymmetric unit of PSAT crystals. The two monomers are related by a twofold noncrystallographic symmetry (Fig. 3A,B). The dimer has an approximate size of 90 × 60 × 60 Å and contains two almost identical monomers with an RMSD of 0.25 Å for 357 C $^{\alpha}$ atoms. The total solvent-accessible area of the dimer is 26,946 Å 2 .

The Protein–Protein Interaction Server (PPIS) (Jones and Thornton 1995, 1996) was used for the analysis of the dimer interface. Approximately 14% of solvent-accessible surface area of each subunit (2228 Å 2) is buried upon dimer formation. Both small and large domains of each monomer provide residues to form the dimer interface. The majority of residues (>80%) is contributed by the large domain. He-

lices $\alpha 1$, $\alpha 2$, $\alpha 3$, $\alpha 4$ of the large domain and loops connecting $\beta 1$ with $\alpha 1$, $\alpha 1$ with $\alpha 2$, $\beta 9$ with $\beta 10$, $\beta 10$ with $\alpha 5$, $\alpha 5$ with $\alpha 6$ and $\alpha 6$ with $\alpha 7$ contain most of the interface residues. The dimer interface is rather flat with a planarity (the RMSD of all the interface atoms from the least-squares plane through the atoms) of 2.4 Å as assessed by PPIS. Interactions between the two monomers are quite extensive. These include a total of 41 polar contacts within 3.8 Å and 164 nonpolar contacts between protein atoms within 5 Å. No ion pairs were found between monomers within a 4.0 Å distance limit. Among all polar contacts, 24 hydrogen bonds were identified. Two PLP molecules located at the dimer interface provide six additional intersubunit hydrogen bonds in total to further stabilize the dimer of PSAT. Moreover, 31 bridging water molecules that have at least one hydrogen bond with each monomer essentially extend the network of interactions at the dimer interface.

More than 8% of the side chains in PSAT dimer (58 in total) are modeled in two alternative conformations. Disordered side chains occur in buried residues and in residues lying on the solvent-accessible surface of the molecule or located close to the dimer interface. Although PSAT monomers superimpose well (see above), about half of the discretely disordered residues in one subunit display only one conformation in the other subunit. These results reflect, most probably, the differences in the microenvironment and molecular interactions of the two monomers in PSAT crystals.

Ion-binding sites

The final model of BALC PSAT contains four Cl^- and four Mg^{2+} ions per dimer. Both ions are present in the crystallization medium at high concentration (see Materials and Methods). Three magnesium ions were modeled at the dimer molecular surface in close proximity to negatively charged side chains of Glu and Asp residues providing direct or water-mediated contacts between symmetry-related molecules in PSAT crystals. The occupancy for one of those Mg^{2+} ions was set to 0.5 based on analysis of isotropic equivalent B -factors. Two sites were modeled for a magnesium ion bound to the side chain of His288 from subunit B. The side chain of this residue adopts at least two alternative conformations. In contrast to magnesium ions, two chloride ions in each monomer are bound inside the protein molecule close to the active site residue Trp102. The binding site for one Cl^- ion is formed by main-chain amides of Ser101, Trp102, Thr152, and Ile153. A water molecule situated within a 3.1 Å distance to a chloride ion mediates additional contacts. The second Cl^- ion is bound in the active site of each monomer between positively charged side chain of Arg334 and the $\text{N}^{\epsilon 1}$ atom of Trp102. The possible role of this ion will be discussed below.

Active site

PSAT dimer contains two structurally identical active sites situated at the dimer interface (Fig. 3A). The distance between the $\text{C4}'$ atoms of the two PLP molecules is 28.7 Å. Residues from both domains of one monomer and the large domain from the second monomer form each active site.

The PLP molecule in the active site is bound to the N^{ζ} atom of Lys196 side chain through a Schiff base linkage (Fig. 4). A prominent stacking interaction characterized by almost absolute parallel alignment of aromatic rings with a separation distance of 3.6 Å is observed between the pyridine ring of PLP and the indole ring of Trp102 on the *re* side of the cofactor. Ser174 and a water molecule that is hydrogen-bonded between O^{γ} of Ser174 and O4P of PLP occupy the *si* side of the cofactor. The methyl group of Ala76 also provides van der Waals interaction with the pyridine ring on the *si* side. The phosphate group of PLP forms hydrogen bonds with N of Ala76, N and O^{γ} of Ser77, $\text{N}^{\epsilon 2}$ of Gln195, $\text{N}^{\delta 2}$ of Asn237* and N and $\text{O}^{\gamma 1}$ of Thr238* (Fig. 4). Additional contacts of the phosphate moiety mediated by three water molecules further improve the anchoring of PLP molecule in the active site. The N1 atom of the pyridine ring forms a hydrogen bond with $\text{O}^{\delta 2}$ of Asp172. The position of Asp172 side chain is stabilized by a water-mediated contact with the side chain of Thr148 and three hydrogen bonds with O^{γ} of Ser174 and main-chain amides of Met173 and Ser174. The $\text{O3}'$ atom of PLP forms a hydrogen bond with

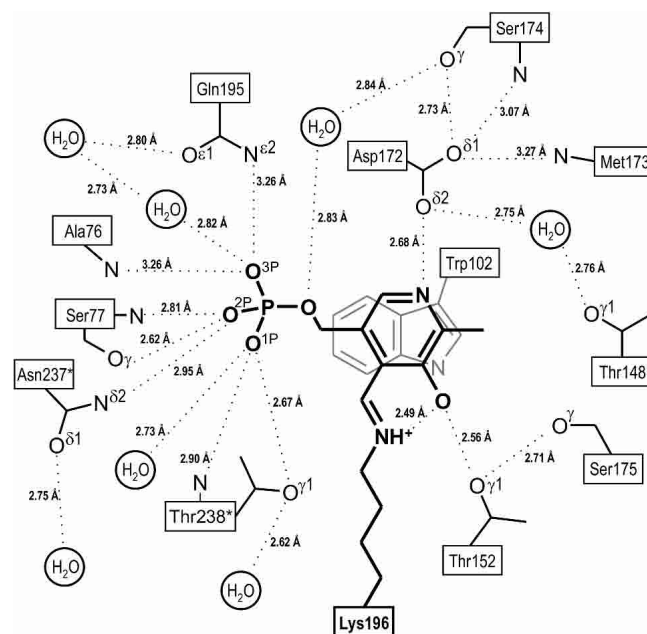


Figure 4. Key interactions of PLP in the active site of BALC PSAT. PLP molecule and the side chain of Lys196 are presented in bold. Hydrogen bonds are shown as dotted lines and their length is indicated. Residues marked with an asterisk originate from the opposite subunit. The figure was produced using ISIS/Draw (MDL, Inc.).

O^γ of Thr152. The side chain of Thr152 is kept in place by hydrogen bond with O^γ of Ser175. Thus, in addition to the internal aldimine bond with Lys196 and stacking interaction with Trp102, PLP is tightly bound in the active site cleft through a total of nine direct hydrogen bonds.

The PLP–Lys196 Schiff base in BALC PSAT has the imine pK_a value of 9.18 ± 0.2 as was determined by spectrophotometry (data not shown). The protein was crystallized at pH 7.5; thus, the internal aldimine is expected to be almost completely protonated under such conditions as indicated also by the deep yellow color of BALC PSAT crystals. It was suggested for aspartate aminotransferase (AAT) from *E. coli* (Hayashi et al. 1998; Mizugushi et al. 2001) that the imine bond and the pyridine ring reside in the same plane in the protonated Schiff base, while deprotonation is accompanied by disruption of planarity due to rotation around the C3–C4–C4′–N^ε torsion angle (χ) (Fig. 5). In the present structure the internal aldimine bond is not absolutely coplanar to pyridine ring with a χ angle of 34.3 ± 0.3° and ~1 Å distance between the N^ε atom and the ring's plane. However, the distance between the imine N and the O3′ atom of PLP (2.5 Å) suggests the formation of a hydrogen bond, which can stabilize the protonated state of internal aldimine (Hayashi et al. 1998). Analysis of more than 20 atomic coordinates of PLP-containing enzymes in the Protein Data Bank (<http://www.rcsb.org>), which have been refined to a resolution better than 2.0 Å, showed that the imine N is lying out of the pyridine ring plane in most of the structures. The conformation of the imine bond is far from absolutely coplanar even when proteins were crystallized from acidic environment with pH 4.3–6.5, which is often much lower than the imine pK_a values and, thus, leads to almost complete protonation of the internal aldimine (Krupka et al. 2000; Ura et al. 2001; Noland et al. 2002). Our results are consistent with those obtained for cystalysin from *Treponema denticola* (Krupka et al. 2000). Although the Schiff base in cystalysin is fully protonated already at pH 8.0 and the protein was crystallized at pH 6.5, the χ angle in the final structure is 50°–60°. Similar results

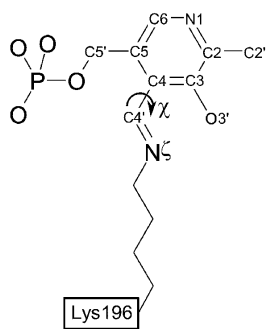


Figure 5. Definition of torsion angle for the internal aldimine bond and atom names in pyridoxal-5′-phosphate. The figure was produced using ISIS/Draw (MDL, Inc.).

(χ = 43°) were obtained also in crystallographic studies of ArnB aminotransferase from *Salmonella typhimurium* crystallized at pH 5.5 (Noland et al. 2002). The two monomers of AAT from *Thermus thermophilus* show χ angles of 28° and 63°, respectively, despite that the crystals were grown at pH 4.3 (Ura et al. 2001), which is generally lower than the imine pK_a value of any aminotransferase (Matsui et al. 2000). There is no clear explanation for such disagreement of the expected and present conformation of the internal imine bond in the active site of BALC PSAT and other PLP-dependent enzymes. We assume that the protonated imine bond in BALC PSAT cannot become absolutely coplanar to pyridine ring, possibly due to stereochemical limitations.

Comparison with other PSAT structures

BALC PSAT displays 40% and 57% sequence identity and 62% and 75% sequence similarity with ECOLI and BCIR PSAT, respectively. The RMSD between C^α atoms after superposition of monomers is 1.1 Å and 0.8 Å for ECOLI and BCIR PSAT, respectively. The relationship between the two domains in a monomer of BALC PSAT estimated using the FIT program (<http://bioinfo1.mbfys.lu.se/~guoguang/fit.html>) differs by ~5° and ~2.5° in comparison to ECOLI and BCIR PSAT, respectively. The relative position of the two subunits that constitute the dimers of BALC and ECOLI PSAT differs by ~6.5°, while the corresponding value for BALC and BCIR psat is less than 2°.

The secondary structure elements are generally similar in all PSAT structures. However, certain differences were found after structure-based alignment of the three proteins (Fig. 6). A surface loop (residues 122–131, according to the numbering in Fig. 6) localized close to the domains interface is the most deviating region. Residues from this loop form two extra β-strands (residues 122–125 and 127–130) in ECOLI PSAT. In both BALC PSAT and BCIR PSAT, these strands are substituted by a 3₁₀ helix and a randomly coiled loop, respectively. The enzyme from *E. coli* contains one shortened β-strand (residues 145–147) corresponding to β5 in BALC and BCIR PSAT. Other differences are related to α-helices. One 3₁₀ helix in ECOLI and BCIR PSAT is transformed into short helix α5 in BALC PSAT. Residues 306–318 in ECOLI PSAT are packed into a 3₁₀ helix followed by an α-helix, while the corresponding residues in both PSATs from *Bacillus* form a long helix (α9).

Loop 122–131 displays low sequence similarity and high structural deviation between BALC and ECOLI PSAT (Fig. 6). In the latter, the corresponding loop contains an insertion of one amino acid residue and protrudes about 10 Å away from the protein (Fig. 7A). Superposition of the two proteins revealed several more regions with high conformational differences. All C^α atoms in the 158–167 loop do not superimpose well, and it also contains one residue insertion. Loops 86–94 and 213–225 packed against each other in the

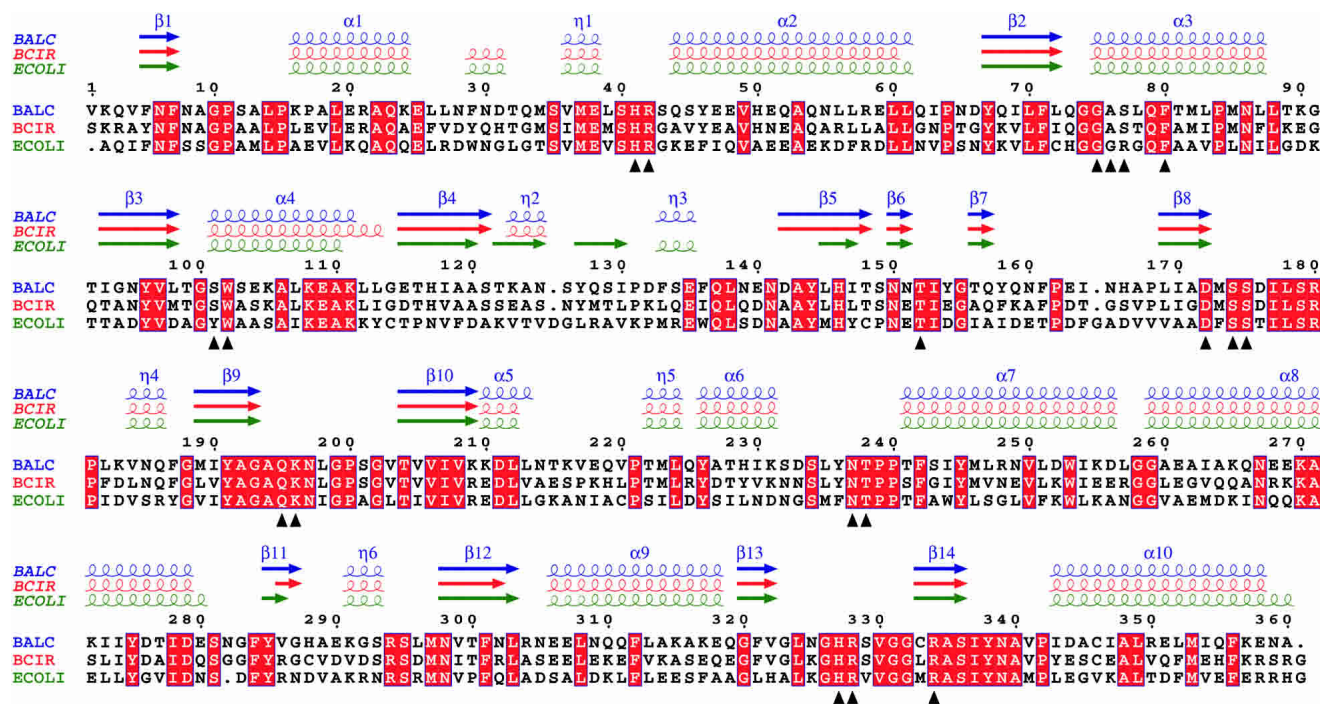


Figure 6. Structural alignment of PSAT from *B. alcalophilus* (BALC), *B. circulans* (BCIR), and *E. coli* (ECOLI). Identical residues are shown in red boxes. The residues are numbered as in the BALC PSAT model. Secondary structure elements for BALC, BCIR, and ECOLI PSAT are presented in blue, red, and green, respectively; helices (α), strands (β), and 3_{10} helices (η) are labeled for BALC PSAT. Active site residues are labeled with triangles. The figure was produced using ESPrnt (Gouet et al. 1999).

large domain create a highly deviating region on the surface of the monomer close to the dimer interface with RMSD of 3.0 Å and 3.1 Å, respectively. Residues 219–225 are directly involved in the interaction between the two monomers. Despite structural similarity of BALC and BCIR PSAT (Fig. 7B), several regions in the two proteins do not superimpose well, and display an RMSD of 2.1 Å (residues 61–65), 2.3 Å (residues 123–140), 1.8 Å (residues 214–219), and 2.2 Å (residues 327–332). Interestingly, significant differences in the secondary structure and loops with altered conformations described above mainly occur on the molecular surface, while the active site loops are structurally more conserved in the three PSAT structures. Eighteen residues surrounding PLP can be superimposed well with an RMSD for C α atoms of 0.3–0.4 Å.

Despite the fact that the three PSAT structures contain almost the same number of amino acid residues, ECOLI PSAT displays a slightly bigger solvent accessible area for monomer and dimer in comparison to both BALC and BCIR PSAT (Table 2). The latter has significantly smaller surface, but its molecular volume is also decreased. The ratio of surface area to volume is almost invariant among the three PSAT models. A similar correlation—e.g., a smaller molecular surface—was found in comparing the extremely alkaliphilic M-protease that displays optimum activity at pH 12.3 (PDB entry 1MPT) (Shirai et al. 1997) to

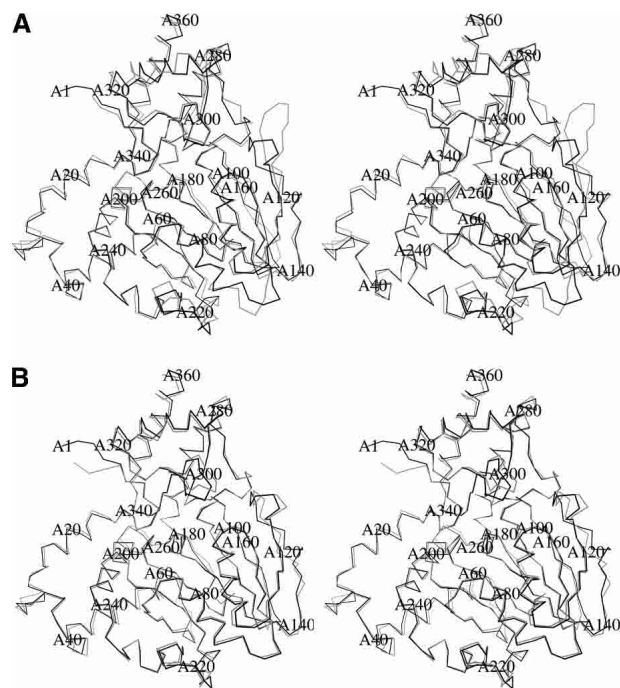


Figure 7. Stereo diagrams of superimposed C α traces of PSAT monomers. (A) BALC (black) and ECOLI PSAT (gray). (B) BALC (black) and BCIR PSAT (gray). Every 20th position in BALC PSAT is labeled. The figure was produced using BOBSCRIPT (Esnouf 1997).

Table 2. Comparison of molecular surface and volume of PSAT

	Amino acid residues		Solvent-accessible surface, Å ²		Volume, Å ³	
	Monomer	Dimer	Monomer	Dimer	Monomer	Dimer
BALC PSAT	360 (357 ^a)	717	15,736	26,946	69,470	134,600
BCIR PSAT	358	716	15,156	25,897	66,430	128,500
ECOLI PSAT	359	718	16,086	27,532	69,560	134,800

^a Number of residues in subunit B.

the less alkaliphilic subtilisin Carlsberg (PDB entry 1SBC) that has maximum activity at pH 10.0 (Neidhart and Petsko 1988). However, due to smaller volume of M-protease, the surface/volume ratio for the two proteases is the same with less than 2.5% difference. Thus, the decrease in molecular surface may contribute to structural adaptation of proteins to alkaline pH, while increased compactness may not play a significant role in contrast to what has been shown for thermophilic proteins (Hough and Danson 1999; Demirjian et al. 2001; Sterner and Liebl 2001). Analysis of intermolecular cavities using VOIDOO (Kleywegt and Jones 1994b) has confirmed the idea that increased compactness is not implemented in alkaline adaptation of PSAT. Both BALC and ECOLI PSAT monomers contain six cavities with a total volume of 42.5 Å³ and 57.4 Å³, respectively. In BCIR PSAT, only three cavities were detected with a total volume of 58.6 Å³.

Surface comparison

Changes in amino acid content on the solvent-accessible surface were detected in proteins adapted to extreme temperatures (Hough and Danson 1999; Demirjian et al. 2001; Sterner and Liebl 2001; Feller 2003), high salinity (Hough and Danson 1999; Demirjian et al. 2001) and acidic pH (Fushinobu et al. 1998; Schäfer et al. 2004). We have analyzed the surface distribution of amino acid residues in PSAT dimers to check whether any correlation with alkaline adaptation can be found. The results are presented in Figure 8 and Table 3. The total number of charged residues on the surface does not differ significantly among BALC, BCIR, and ECOLI PSAT. However, the ratio between surface residues with negative and positive charges has been considerably changed in alkaliphilic PSAT. Indeed, more acidic residues are exposed in both BALC and BCIR PSAT, while basic residues prevail on the surface of mesophilic enzyme from *E. coli* (Fig. 8). A bigger difference between negative and positive residues is observed in PSAT from the obligatory alkaliphile *B. alcalophilus* in comparison to the enzyme from the facultative alkaliphile *B. circulans*. This may explain the slightly higher value of the experimentally determined isoelectric point of BALC PSAT (pI ~4.73) in comparison to BCIR PSAT (pI ~4.55). ECOLI PSAT contains

much fewer Glu residues on the surface, but the presence of Asp residues is increased compared to BCIR and BALC PSAT (Table 3). The number of uncharged polar residues is elevated in BALC PSAT. Nonpolar residues are highly presented on the surface of ECOLI PSAT, while their number in BCIR and BALC PSAT is decreased compared to ECOLI PSAT by 37% and 55%, respectively (Fig. 8). Thus, our results suggest that reorganization of the molecular surface by predominance of negatively charged residues and decreased number of hydrophobic residues may be required for alkaline adaptation of PSAT. Such adaptation mechanism seems to be specific for PSAT, since in alkaline proteases of the subtilisin family the more alkaliphilic enzymes contain an excess of positively charged residues on their surface (Shirai et al. 1997). Similarly, contradictory results were previously obtained for acidophilic proteins. More negative residues were found on the surface of the extremely acidophilic xylanase from *Aspergillus kawachii* (Fushinobu et al. 1998), while the balance of charged residues is opposite in the acidophilic maltose-binding protein from *A. acidocaldarius* (Schäfer et al. 2004). These data suggest that the changes in the ratio of negative and positive charges on the molecular surface as a mechanism of protein adaptation to different pH environments are specific for each class of proteins.

The relative excess of Glu and shortage of Asp residues on the surface of both BALC and BCIR PSAT in compari-

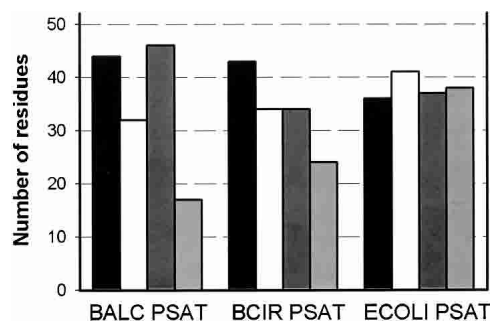


Figure 8. Content of amino acid residues on the molecular surface of PSAT dimers. Black bars represent negatively charged residues (Asp and Glu); white bars, positively charged residues (Arg and Lys); dark gray bars, polar uncharged residues (Asn, Gln, His, Ser, and Thr); light gray bars, hydrophobic residues (Ala, Gly, Ile, Leu, Phe, Pro, and Val).

Table 3. Amino acids content on the surface of PSAT

Residues	BALC	BCIR	ECOLI
R	6	14	15
K	26	20	26
E	34	30	12
D	10	13	24
All charged	76	77	77
Q	20	14	12
N	20	6	12
T	1	2	8
A	4	12	16
H	—	6	—
V	3	2	8
S	5	6	5
L	2	—	—
P	5	—	2
I	—	—	2
F	—	—	2
G	3	10	8

Surface residues were assessed by the Swiss-PdbViewer (Guex and Peitsch 1997), as described in Materials and Methods.

son to ECOLI PSAT (Table 3) prompted us to analyze the length of the side chains present on the surface of the proteins. All surface residues were subdivided into two categories, depending on the number of atoms in the side chain. The first category includes residues whose side chain contains four or less atoms (“short” side chain), while those with a longer side chain belong to the second category. The residues without a side chain (Gly) and those with a rigid one (Pro) were excluded from the calculations. Interestingly, the percentage of residues with a “short” side chain is decreased from 53% in ECOLI PSAT to 33% and 30% in BCIR and BALC PSAT, respectively. To the best of our knowledge, adaptation mechanisms involving the length of the side chains on the molecular surface were not previously reported for any group of extremophilic proteins. It is not possible at the time to conclude whether the above-described preference for surface side chains is related to alkaline adaptation, or if it reflects an evolutionary difference between PSATs from the three species. To be more clarified, this issue needs further consideration.

Molecular contacts

We have analyzed the total number of interactions in PSAT monomer and the contacts at the dimer interface and between small and large domains in a monomer. The results are summarized in Table 4. The most striking difference between the three PSAT models was found in ion pairs. In comparison to ECOLI PSAT, the total amount of salt bridges in a monomer decreases to 64% and 55% in BCIR and BALC PSAT, respectively. Two ion pairs in each monomer of ECOLI PSAT are involved in interaction between the small and large domain, while they are absent in both BALC and BCIR PSAT. Only the enzyme from *B. circulans* contains two Arg-Glu hydrogen-bonded ion pairs at the dimer interface. Upon dimer formation most of the salt bridges in all three PSAT structures remain on the molecular surface. In total, 16, 22, and 40 ion pairs were detected on the surface of dimeric BALC, BCIR, and ECOLI PSAT, respectively. In addition, differences in the character of interaction between charged residues were found between mesophilic PSAT from *E. coli* and PSAT from both facultative and obligatory alkaliphiles. These residues in ECOLI PSAT dimer form in total 11 ion networks that include from three to six cross-interacting charged residues. Most of these networks are exposed to the solvent. Notably, only two such ion networks were found in BALC PSAT dimer and four in BCIR PSAT. Thus, reduced number of ion networks on the molecular surface together with decreased total amount of ion pairs and solvent exposed ion pairs may contribute to alkaline adaptation of PSAT. However, results obtained by Shirai et al. (1997) suggested an increased number of ion pairs correlated with alkaline adaptation of M-protease. Moreover, no significant changes in the amount of ion pairs were found in alkaline cellulase K compared to mesophilic cellulases (Shirai et al. 2001). Taken together, these observations suggest that the mechanisms of alkaline adaptation involving balance of ion interactions are not universal among all proteins, but they appear to be specific for each enzyme class.

In contrast to the increased number of ion pairs, less hydrogen bonds per monomer were identified in mesophilic

Table 4. Comparison of interactions between BALC, BCIR, and ECOLI PSAT

	Interface between the small and large domains			Dimer interface			All contacts in a monomer		
	BALC	BCIR	ECOLI	BALC	BCIR	ECOLI	BALC	BCIR	ECOLI
No. of nonpolar contacts ^a	89	77	63	164	189	136	1928	2008	1949
No. of H-bonds	25	23	23	24	26	18	464	489	408
No. of ion pairs ^b	—	—	2	—	2	—	12	14	22
No. of other polar contacts ^c	14	16	17	17	16	22	446	376	398

Only contacts between protein atoms were calculated. Subunit A was used for calculations.

^a Number of atom pairs of aliphatic or aromatic carbons within 5.0 Å.

^b Number of residue pairs in which negatively and positively charged atoms exist within 4.0 Å.

^c Number of atom pairs in which O or N atoms exist within 3.8 Å excluding H-bonds and ion pairs.

ECOLI PSAT. The number of hydrogen bonds is increased in BALC and BCIR PSAT by 14% and 20%, respectively (Table 4). Similar results were previously shown for the extremely alkaliphilic M-protease in comparison to the less alkaliphilic subtilisin Carlsberg (Shirai et al. 1997). Interestingly, an increase in the amount of hydrogen bonds is similar for these two groups of unrelated enzymes, proteases, and aminotransferases. This involvement of hydrogen bonds, and in particular the similar quantitative relationships observed for the two groups of proteins, strongly suggests that an increase in hydrogen bonding might constitute an important mechanism for structural adaptation of a variety of proteins to an alkaline environment. However, applicability of this mechanism to other alkaliphilic proteins remains to be established.

As mentioned above, unlike the *E. coli* enzyme, the interactions between the small and large domain in BALC and BCIR PSAT do not involve ion pairs. More hydrophobic interactions between the two domains were detected in BALC and BCIR PSAT compared to ECOLI PSAT (Table 4). The number of hydrogen bonds and other polar contacts between the two domains is similar among the three PSATs.

The interactions at the dimer interface differ quite significantly between BALC, BCIR, and ECOLI PSAT (Table 4). The enzymes from both alkaliphilic *Bacillus* species contain additional hydrogen bonds at the interface. In comparison to ECOLI PSAT, the number of hydrogen bonds in BALC and BCIR PSAT is increased by 33% and 44%, respectively. Furthermore, the total amount of nonpolar contacts at the dimer interface is increased in BALC and BCIR PSAT by 21% and 39%, respectively, while the number of other polar contacts (except hydrogen bonds and ion pairs) is decreased by 27% and 23%. Thus, the interaction between the two monomers in more alkaliphilic PSAT is enhanced by additional hydrophobic contacts and replacement of some weak polar contacts by stronger hydrogen bonds. As dimerization is required for enzymatic activity of PSAT, such changes in interactions at the dimer interface may be important in alkaline adaptation.

Active site comparison

The pH optima of the enzymatic activity of BALC (Fig. 1) and BCIR PSAT (pH 9.0; E.G. Kapetaniou, A.P. Dubnovitsky, and A.C. Papageorgiou, unpubl.) are shifted to alkaline pH in comparison to ECOLI PSAT (Kallen et al. 1987). The pK_a values of the internal aldimine in BALC PSAT (pK_a 9.2) and BCIR PSAT (pK_a ~9.0) (data not shown) are also higher than that for ECOLI PSAT (pK_a 8.4) (Hester et al. 1999). Thus, in addition to changes concerning the whole protein molecule, there should be certain differences in the active site providing BALC and BCIR PSAT with an elevated activity at alkaline pH. Analysis of the molecular contacts and relative position of PLP mol-

ecule in the active site of three PSAT has revealed structural features possibly related to alkaline adaptation.

The residues Ala76 and Ser77 in both PSAT from *Bacillus* replace residues Gly76 and Arg77 in ECOLI PSAT (Fig. 9). This leads to the rearrangement in hydrogen bonding of the PLP phosphate moiety. The N and O^γ atoms of Ser77 and the N of Ala76 form hydrogen bonds with nonester oxygen atoms of PLP (Fig. 4). In ECOLI PSAT the N atom of Arg77 forms one hydrogen bond, while the main-chain amide of Gly76 forms hydrogen bonds with two oxygen atoms of the phosphate moiety (Hester et al. 1999). Moreover, C^β atom of Ala76 in BALC and BCIR PSAT provides a van der Waals interaction with the pyridine ring of the cofactor. This interaction is missing in ECOLI PSAT. Residue Gln73 in BALC PSAT (Gln74 in BCIR PSAT) provides a water-mediated contact to the phosphate moiety of PLP, while in ECOLI PSAT this position is occupied by His residue, which is not involved in cofactor binding. Another distinctive feature of BALC and BCIR PSAT is a hydrogen bond between the $O^{\gamma 1}$ atom of Thr152 (Thr153 in BCIR PSAT) and the $O3'$ atom of PLP (Fig. 4). Such a hydrogen bond does not exist in the unligated ECOLI PSAT (Fig. 9), but is present in its complex with α -methyl-L-glutamate (Hester et al. 1999). The hydrogen bond between Tyr225 and the $O3'$ atom of PLP in aspartate aminotransferase from *E. coli* (AAT) was shown to lower the pK_a of the internal aldimine from 8.5 in Tyr225Phe mutant to 6.8 in the wild-type enzyme (Inoue et al. 1991). Our results suggest an opposite role of the hydrogen bond Thr-PLP in PSAT, since the pK_a values for BALC and BCIR PSAT having Thr-PLP hydrogen bond are higher than the pK_a of the internal aldi-

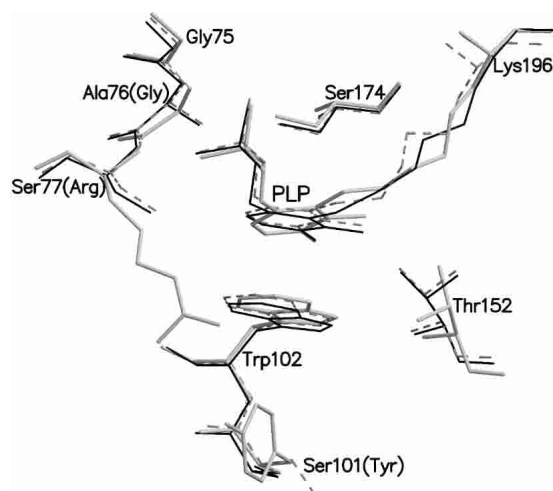


Figure 9. Differences in the active site of BALC (black), BCIR (dashed) and ECOLI (gray) PSAT. Eighteen active site residues were superimposed. Only part of them is shown for clarity of presentation. The residues are labeled for BALC PSAT and ECOLI PSAT (in parentheses) if the residue type is different. The figure was produced using MOLSCRIPT (Kraulis 1991) and Raster3D (Merritt and Murphy 1994).

mine in the unligated ECOLI PSAT, where the structurally equivalent Thr residue does not form an appropriate hydrogen bond.

Except from residue Thr152 there is no other suitable candidate that would potentially affect (increase) the pK_a of the internal aldimine in BALC and BCIR PSAT. There is no evidence that the Cl^- ion bound between the side chain of Arg334 and $N^{\epsilon 1}$ atom of Trp102 in BALC PSAT plays any role, since it was not found in BCIR PSAT and the two enzymes still have close pH optima and imine pK_a values. Moreover, binding of a sulfate anion in the same position was previously found in AAT from *E. coli* (PDB entry 1ASF). Thus, interaction of Thr152 side chain with the $O3'$ atom of the cofactor in PSAT might be responsible for the alkaline shift of enzymatic activity, although it has to be tested by site-directed mutagenesis analysis.

Changes in the microenvironment of PLP lead to slightly different relative positions of the cofactor in the active sites of the three PSATs. The pyridine ring of PLP in ECOLI PSAT stacks to the indole ring of Trp102 with a -9° inclination angle, and there is an additional aromatic Tyr residue on the other side of Trp indole ring positioned perpendicularly to the latter (Fig. 9). In BALC PSAT the aromatic rings of Trp102 and PLP are almost absolutely parallel, while the two rings are angled at about 2.5° in BCIR PSAT. The residue Ser101 in both PSAT from *Bacillus* replaces the Tyr101 in ECOLI PSAT. In contrast to PLP, the planes of the Trp indole rings are nearly parallel in the three superimposed PSAT models. The more parallel alignment of the aromatic rings can increase the electron withdrawing effect of the cofactor and favor the formation of the quinoid intermediate (Ford et al. 1980; Hayashi et al. 1990; John 1995). However, changes in the relative position of PLP in the active site are unlikely to shift the pK_a value of the internal aldimine or the enzyme's pH optimum, although such a possibility cannot be ruled out without direct experimental evidence.

Conclusions

The crystal structure of PSAT from the obligate alkaliophile *B. alcalophilus* has been determined to atomic resolution (1.08 Å). The pH optimum of BALC PSAT enzymatic activity is shifted to alkaline pH in comparison to ECOLI PSAT. The structure of BALC PSAT was compared to the structure of ECOLI PSAT and to that of PSAT from a facultative alkaliphile *B. circulans* subsp. *alkalophilus*. A number of distinctive structural features that might be implicated in the alkaline adaptation of BALC PSAT were identified. Two active site residues directly interacting with the PLP molecule (Gly76 and Arg77 in ECOLI PSAT) are replaced in BALC and BCIR PSAT with Ala and Ser, respectively. There is no hydrogen bond between $O^{\gamma 1}$ atom of Thr153 and $O3'$ atom of PLP in ECOLI PSAT, although it

exists in BALC and BCIR PSAT. Such changes in the PLP microenvironment may contribute to different relative position of the cofactor in the active site and result in better parallel alignment between the PLP pyridine ring and the indole ring of Trp102 in BALC PSAT. The hydrophobic interaction between the small and the large domain is enhanced in the alkaliphilic enzymes from *Bacillus* species. More nonpolar contacts and hydrogen bonds but fewer weak polar contacts are present at the dimer interface in BALC and BCIR PSAT. Differences in the relative position of the two monomers in PSAT dimer and between the two domains in a monomer are greater for BALC and ECOLI PSAT than for BALC and BCIR PSAT. The total number of hydrogen bonds in a monomer is increased in BALC and BCIR PSAT compared to ECOLI PSAT. The mesophilic PSAT enzyme from *E. coli* contains significantly increased amount of ion pairs, which in turn, form a number of ion networks. The number of such networks is decreased in both BALC and BCIR PSAT. The solvent-accessible surface of BALC and BCIR PSAT is reduced. However, the surface per volume ratio is almost invariant for the three PSAT structures. Fewer hydrophobic residues were found on the surface of BALC and BCIR PSAT than in ECOLI PSAT. More positively charged residues are exposed on the surface of ECOLI PSAT, while an excess of negatively charged surface residues was found in BALC and BCIR PSAT. A preference for surface residues with long side chains was identified in BALC and BCIR PSAT compared to ECOLI PSAT. In addition, a surface loop (residues 122–131) adopts a remarkably different conformation in BALC, BCIR, and ECOLI PSAT. In the latter, this loop is better ordered due to the formation of two additional β -strands. Another β -strand is shortened in ECOLI PSAT in comparison to BALC and BCIR PSAT. Structural features mentioned above might therefore constitute factors responsible for the adaptation of PSAT to alkaline pH. Site-directed mutagenesis studies could establish the precise role of the aforementioned structural features in the alkaline adaptation of the PSAT enzymes. Work toward this direction is under way.

Materials and methods

Purification and crystallization

Recombinant BALC PSAT was expressed in *E. coli* cells, purified, and crystallized using the hanging-drop vapor diffusion method as described (Dubnovitsky et al. 2003). Briefly, up to 150 μm thick, plate-like crystals were obtained at 16°C with 30–35 mg/mL protein solution and mother liquor consisting of 30% (v/v) PEG 400, 0.2 M magnesium chloride hexahydrate, 0.1 M HEPES (pH 7.5). These crystals usually have 0.4° – 0.6° mosaicity and diffract to 1.3–1.5 Å resolution using synchrotron radiation. Modification of crystallization conditions by addition of 7.5% (v/v) glycerol decreased crystal mosaicity (0.2° – 0.4°) and extended the diffraction limit to ~ 1.0 Å resolution. Final mother liquor contained 27.75%

(v/v) PEG 400, 185 mM magnesium chloride hexahydrate, 7.5% (v/v) glycerol, and 92.7 mM HEPES (pH 7.5). Crystals obtained with or without glycerol belong to the orthorhombic space group $P2_12_12$ and contain one dimer in the asymmetric unit. BCIR PSAT was crystallized based on a previously reported crystallization protocol (Moser et al. 1996).

Enzymatic activity assay

Enzymatic activity of PSAT was determined using a previously described coupled assay (Hirsch and Greenberg 1967) with modification. Instead of the nonspecific L-glutamate dehydrogenase (GLDH, EC 1.4.1.3) from bovine liver, NADP-dependent GLDH (EC 1.4.1.4) from *Proteus* sp. was used due to its higher activity at pH above 9.0. The activity assay was carried out using 0.3 μg of PSAT in 1 mL of reaction mixture containing 0.5 mM 3-phosphohydroxypyruvate, 8 mM glutamate, 32 mM ammonium acetate, 0.25 mM NADPH, 20 μM pyridoxal-5'-phosphate, 10 U GLDH (grade II, Toyobo) in 100 mM HEPES (pH 7.0–8.2) or CHES (pH 8.5–10.0). Reaction was started by addition of 3-phosphohydroxypyruvate and the decrease in NADPH absorption at 340 nm was measured at 25°C.

Diffraction measurements and data processing

Two data sets at 1.4 Å and 1.08 Å resolution were collected from single crystals on beamlines X11 and BW7A at EMBL Hamburg using MAR CCD detectors at wavelengths of 0.811 Å and 0.9007 Å, respectively. Crystals were flash-cooled in a cryo-stream at 100 K without additional cryoprotection. To record a wide range of intensities, high- and low-resolution reflections for each data set were collected separately with different exposure times and oscillation ranges. Data were processed with the HKL program suite (Otwinowski and Minor 1997). The TRUNCATE program (Collaborative Computational Project 4 1994) was used to convert intensities to amplitudes. Data processing statistics are summarized in Table 1.

Structure determination and refinement

Data set I (1.4 Å) was used for the initial structure determination and data set II (1.08 Å) was used in the final refinement (Table 1). The structure of BALC PSAT was determined by molecular replacement using the program AMoRe (Navaza 1994). A polyalanine model of subunit A from the ECOLI PSAT structure at 2.3 Å resolution (Hester et al. 1999) was used as a search model. Using data in the range 8–3 Å, a list of 68 rotation solutions was obtained with the first two peaks 1.2σ higher than the next one, showing 6.7% and 6.3% correlation coefficient, respectively. The top peak was used in the translation function, and after rigid body refinement it showed a correlation coefficient of 30.0% and an R -factor of 55%. Due to the presence of two molecules in the asymmetric unit, the position of the first molecule was fixed in the translation search for the second molecule. Finally, a correlation coefficient of 38.6% and an R -factor of 51% were obtained for two solutions after rigid body refinement with AMoRe. Examination of coordinates using the program O (Jones et al. 1991) revealed that the obtained solutions represent subunits A and B from different dimers. Visualization of crystallographic symmetry-related monomers allowed us to reconstitute dimeric PSAT molecule that showed good crystal packing.

Tight ncs-restraints (200 kcal/mol·Å²) were applied in the initial refinement steps at 1.4 Å resolution and were released in the refinement against the 1.08 Å data. A set of 5% randomly selected reflections was excluded from the refinement and was used to calculate the free R -factor (R_{free}) (Brunger 1997). The solution from AMoRe was subjected to rigid body and simulated annealing refinement using CNS (Brunger et al. 1998) that resulted in an R_{cryst} of 44.5% and an R_{free} of 46.1%. After map averaging using DM from the CCP4 program package (Collaborative Computational Project Number 4 1994) the resulting map showed good connectivity throughout the polypeptide chain. Electron density for ~40% of the side chains was easily interpretable according to the amino acid sequence. Good electron density for PLP molecules was present in both active sites of the enzyme. Thus, two PLP molecules were added to the model in the beginning of the refinement. More than 95% of the side chains were added after several rounds of manual rebuilding using the program O followed by simulated annealing refinement. The R_{cryst} and R_{free} values dropped to 27% and 27.9%, respectively.

The resolution was extended to 1.08 Å (from 1.4 Å) in steps of 0.1 Å using simulated annealing refinement. Further refinement was carried out using the restrained conjugate least-squares method as implemented in SHELX-97 (Sheldrick and Schneider 1997). XtalView (McRee 1999) was used for manual modeling. Stereochemical restraints to bond lengths and angles, chiral volumes, and planar groups were applied during the refinement as well as additional restraints to anisotropic displacement parameters of bonded atoms. Default effective standard deviations were used for all the restraints. The restraints for PLP were released at the final stage of the refinement. The model was treated isotropically at the first five cycles of the refinement. Anisotropic refinement of temperature factors for all nonhydrogen atoms remarkably improved the electron density map and resulted in decreased R_{cryst} and R_{free} values by 3.9% and 3.0%, respectively. In most cases, proper positions of carbon, nitrogen, and oxygen atoms could be determined.

Water molecules were added using an automated water divining procedure as implemented in SHELX-97 and were systematically checked in the graphics before they were included in the refinement. Water molecules with temperature factors greater than 60 Å² were excluded from subsequent refinement. Half-occupied solvent sites were modeled within hydrogen-bonding distances to the side chains in double conformations. Multiple conformations were built for ~8% of the side chains in each monomer. Due to the absence of sufficient electron density residues 214–216 from subunit B were excluded from the model at this stage, and residues 215, 216, 218, and 219 from subunit A and 218 from subunit B were modeled as alanine residues.

Four prominent electron density peaks with spherical shape were interpreted as Mg²⁺ ions based on their presence in the crystallization medium. Two ions are bound to the side chains of Asp and Glu residues within distance typical for magnesium ions displaying distinctive coordination sphere (Harding 2001). One Mg²⁺ ion is bound between the side chains of Asp and Glu residues making only water-mediated contacts with both side chains and a symmetry related molecule. Two sites were modeled for one magnesium ion in proximity to discretely disordered side chain of His288 from subunit B. Four other peaks (>10 σ) were interpreted as chloride ions whose concentration in the mother liquor is close to 0.4 M. Based on the shape of electron densities in $|F_o| - |F_c|$ map, one HEPES molecule with half occupancy, one glycerol molecule, and four PEG molecules with different polymer content were included in the final model. Several more electron densities for PEG molecules were visible in the $|F_o| - |F_c|$ map, but were not modeled

due to poorly defined electron density reflecting, most probably, low occupancy.

Hydrogen atoms at riding positions were added after the refinement had converged to an R_{cryst} of 12.7% and an R_{free} of 15.3%. Those hydrogens attached to the terminal O and N atoms or to the side chains of histidine residues were ignored. Addition of hydrogen atoms resulted in 1.0% and 1.3% drop in the R_{cryst} and R_{free} , respectively. At the final step, refinement was performed against all crystallographic data, including the test set.

Structure analysis

The quality of the model was checked using PROCHECK (Laskowski et al. 1993). The RMSD from ideal geometry and Luzzati plot were calculated by SHELX (Sheldrick and Schneider 1997). LSQMAN (Kleywegt and Jones 1994a) was used for structural superposition and calculation of RMSD for particular loops. Cavities inside the protein molecule were analyzed using VOIDOO (Kleywegt and Jones 1994b) with a probe radius of 1.2 Å and minimal cavity volume of 5 Å³. Molecular volume was calculated by VOIDOO (Kleywegt and Jones 1994b) using a probe radius of 1.4 Å. The area of solvent-accessible surface was calculated with program SURFACE (Collaborative Computational Project Number 4 1994) using a probe radius of 1.4 Å and ZSTEP of 0.1. Hydrogen bonds were assessed by CONTACT (Collaborative Computational Project Number 4 1994) using ANGLE instruction and 3.3 Å distance limit. Secondary structure elements were analyzed with DSSP (Kabsch and Sander 1983). Structure-based alignment was performed using protein structure comparison service SSM (Krissinel and Henrick 2003) at European Bioinformatics Institute (<http://www.ebi.ac.uk/msd-srv/ssm>) and was visually inspected on graphics. Surface residues, which have >30% accessible surface area assessed in Swiss-PdbViewer (Guex and Peitsch 1997) using the default probe radius were classified as solvent accessible residues.

Protein Data Bank accession codes

Atomic coordinates and structure factors have been deposited with the Rutgers Protein Data Bank under the accession codes 1W23 (BALC PSAT) and 1W3U (BCIR PSAT).

Acknowledgments

This work was supported by the Academy of Finland (grant no. 878699) and the Sigrid Jusélius Foundation. We thank N. Battchikova, M. Koivulehto, and T. Korpela, University of Turku, for generously providing the BALC PSAT plasmid, and the staff at EMBL/DESY, Hamburg, for help and advice during data collection. Access to EMBL/DESY, Hamburg (European Community–Access to Research Infrastructure Action of the Improving Human Potential Programme to the EMBL Hamburg Outstation, contract no. HPRI-CT-1999-00017) is greatly acknowledged.

References

Alexander, F.W., Sandmeier, E., Mehta, P.K., and Christen, P. 1994. Evolutionary relationships among pyridoxal-5'-phosphate-dependent enzymes: Regio-specific α , β and γ families. *Eur. J. Biochem.* **219**: 953–960.

Baek, J.Y., Jun, D.Y., Taub, D., and Kim, Y.H. 2003. Characterization of human phosphoserine aminotransferase involved in the phosphorylated pathway of L-serine biosynthesis. *Biochem. J.* **373**: 191–200.

Basurko, M.J., Marche, M., Darriet, M., and Cassaigne, A. 1999. Phosphoserine

aminotransferase, the second step-catalyzing enzyme for serine biosynthesis. *IUBMB Life* **48**: 525–529.

Brünger, A.T. 1997. Free R value: Cross-validation in crystallography. *Methods Enzymol.* **277**: 366–396.

Brünger, A.T., Adams, P.D., Clore, G.M., DeLano, W.L., Gros, P., Grosse-Kunstleve, R.W., Jiang, J.S., Kuszewski, J., Nilges, M., Pannu, N.S., et al. 1998. Crystallography & NMR system: A new software suite for macromolecular structure determination. *Acta Crystallogr. Sect. D Biol. Crystallogr.* **54**: 905–921.

Collaborative Computational Project Number 4. 1994. The CCP4 suite: Programs for protein crystallography. *Acta Crystallogr. Sect. D Biol. Crystallogr.* **50**: 760–763.

de Koning, T.J., Snell, K., Duran, M., Berger, R., Poll-The, B.T., and Surtees, R. 2003. L-serine in disease and development. *Biochem. J.* **371**: 653–661.

de Lemos Esteves, F., Ruelle, V., Lamotte-Brasseur, J., Quinting, B., and Frere, J.M. 2004. Acidophilic adaptation of family 11 endo- β -1,4-xylanases: Modeling and mutational analysis. *Protein Sci.* **13**: 1209–1218.

Demirjian, D.C., Moris-Varas, F., and Cassidy, C.S. 2001. Enzymes from extremophiles. *Curr. Opin. Chem. Biol.* **5**: 144–151.

Dubnovitsky, A.P., Kapetaniou, E.G., and Papageorgiou, A.C. 2003. Expression, purification, crystallization and preliminary crystallographic analysis of phosphoserine aminotransferase from *Bacillus alcalophilus*. *Acta Crystallogr. Sect. D Biol. Crystallogr.* **59**: 2319–2321.

Esnouf, R.M. 1997. An extensively modified version of MolScript that includes greatly enhanced coloring capabilities. *J. Mol. Graph. Model.* **15**: 132–134.

Feller, G. 2003. Molecular adaptation to cold in psychrophilic enzymes. *Cell. Mol. Life Sci.* **60**: 648–662.

Ford, G.C., Eichele, G., and Jansonius, J.N. 1980. Three-dimensional structure of a pyridoxal-phosphate-dependent enzyme, mitochondrial aspartate aminotransferase. *Proc. Nat. Acad. Sci.* **77**: 2559–2563.

Fushinobu, S., Ito, K., Konno, M., Wakagi, T., and Matsuzawa, H. 1998. Crystallographic and mutational analyses of an extremely acidophilic and acid-stable xylanase: Biased distribution of acidic residues and importance of Asp37 for catalysis at low pH. *Protein Eng.* **11**: 1121–1128.

Gouet, P., Courcelle, E., Stuart, D.I., and Metz, F. 1999. ESPript: Multiple sequence alignments in PostScript. *Bioinformatics* **15**: 305–308.

Grishin, N.V., Phillips, M.A., and Goldsmith, E.J. 1995. Modeling of the spatial structure of eukaryotic ornithine decarboxylases. *Protein Sci.* **4**: 1291–1304.

Guex, N. and Peitsch, M.C. 1997. SWISS-MODEL and the Swiss-PdbViewer: An environment for comparative protein modeling. *Electrophoresis* **18**: 2714–2723.

Harding, M.M. 2001. Geometry of metal–ligand interactions in proteins. *Acta Crystallogr. D Biol. Crystallogr.* **57**: 401–411.

Hayashi, H., Inoue, Y., Kuramitsu, S., Morino, Y., and Kagamiyama, H. 1990. Effects of replacement of tryptophan-140 by phenylalanine or glycine on the function of *Escherichia coli* aspartate aminotransferase. *Biochem. Biophys. Res. Commun.* **167**: 407–412.

Hayashi, H., Mizuguchi, H., and Kagamiyama, H. 1998. The imine-pyridine torsion of the pyridoxal 5'-phosphate Schiff base of aspartate aminotransferase lowers its pKa in the unliganded enzyme and is crucial for the successive increase in the pKa during catalysis. *Biochemistry* **37**: 15076–15085.

Hester, G., Stark, W., Moser, M., Kallen, J., Markovic-Housley, Z., and Jansonius, J.N. 1999. Crystal structure of phosphoserine aminotransferase from *Escherichia coli* at 2.3 Å resolution: Comparison of the unliganded enzyme and a complex with α -methyl-L-glutamate. *J. Mol. Biol.* **286**: 829–850.

Hirsch, H. and Greenberg, D.M. 1967. Studies on phosphoserine aminotransferase of sheep brain. *J. Biol. Chem.* **242**: 2283–2287.

Horikoshi, K. 1999. Alkaliphiles: Some applications of their products for biotechnology. *Microbiol. Mol. Biol. Rev.* **63**: 735–750.

Hough, D.W. and Danson, M.J. 1999. Extremozymes. *Curr. Opin. Chem. Biol.* **3**: 39–46.

Ichihara, A. and Greenberg, D.M. 1957. Further studies on the pathway of serine formation from carbohydrate. *J. Biol. Chem.* **224**: 331–341.

Inoue, K., Kuramitsu, S., Okamoto, A., Hirotsu, K., Higuchi, T., Morino, Y., and Kagamiyama, H. 1991. Tyr225 in aspartate aminotransferase: Contribution of the hydrogen bond between Tyr225 and coenzyme to the catalytic reaction. *J. Biochem.* **109**: 570–576.

Jaenicke, R. and Böhm, G. 1998. The stability of proteins in extreme environments. *Curr. Opin. Struct. Biol.* **8**: 738–748.

Jansonius, J.N. 1998. Structure, evolution and action of vitamin B6-dependent enzymes. *Curr. Opin. Struct. Biol.* **8**: 759–769.

John, R.A. 1995. Pyridoxal phosphate-dependent enzymes. *Biochim. Biophys. Acta* **1248**: 81–96.

Jones, S. and Thornton, J.M. 1995. Protein–protein interactions: A review of protein dimer structures. *Prog. Biophys. Mol. Biol.* **63**: 31–65.

- . 1996. Principles of protein–protein interactions. *Proc. Nat. Acad. Sci.* **93**: 13–20.
- Jones, T.A., Zou, J.Y., Cowan, S.W., and Kjeldgaard, M. 1991. Improved methods for building protein models in electron density maps and the location of errors in these models. *Acta Crystallogr. Sect. A Fundam. Crystallogr.* **47**: 110–119.
- Kabsch, W. and Sander, C. 1983. Dictionary of protein secondary structure: Pattern recognition of hydrogen-bonded and geometrical features. *Biopolymers* **22**: 2577–2637.
- Kallen, J., Kania, M., Markovic-Housley, Z., Vincent, M.G., and Jansonius, J.N. 1987. Crystallographic and solution studies on phosphoserine aminotransferase from *Escherichia coli*. In *Biochemistry of vitamin B6* (eds. P. Christen and T. Korpela), pp. 157–160. Birkhäuser Verlag, Basel, Switzerland.
- Kleywegt, G.J. and Jones, T.A. 1994a. A super position. *CCP4/ESF-EACBM Newslitt. Protein Crystallog.* **31**: 9–14.
- . 1994b. Detection, delineation, measurement and display of cavities in macromolecular structures. *Acta Crystallogr. Sect. D Biol. Crystallogr.* **50**: 178–185.
- Kraulis, P.J. 1991. MOLSCRIPT: A program to produce both detailed and schematic plots of protein structures. *J. Appl. Crystallogr.* **24**: 946–950.
- Krissinel, E. and Henrick, K. 2003. Protein structure comparison in 3D based on secondary structure matching (SSM) followed by C^α alignment, scored by a new structural similarity function. In *Proceedings of the 5th International Conference on Molecular Structural Biology, Vienna, September 3–7, 2003* (eds. A.J. Kungl and P.J. Kungl), p. 88. Austrian Chemical Society, Graz, Austria.
- Krulwich, T.A., Ito, M., Gilmour, R., and Guffanti, A.A. 1997. Mechanisms of cytoplasmic pH regulation in alkaliphilic strains of *Bacillus. Extremophiles* **1**: 163–169.
- Krupka, H.I., Huber, R., Holt, S.C., and Clausen, T. 2000. Crystal structure of cystalysin from *Treponema denticola*: A pyridoxal 5'-phosphate-dependent protein acting as a haemolytic enzyme. *EMBO J.* **19**: 3168–3178.
- Laskowski, R.A., MacArthur, M.W., Moss, D.S., and Thornton, J.M. 1993. PROCHECK: A program to check the stereochemical quality of protein structures. *J. Appl. Crystallogr.* **26**: 283–291.
- Longhi, S., Czjzek, M., and Cambillau, C. 1998. Messages from ultrahigh resolution crystal structures. *Curr. Opin. Struct. Biol.* **8**: 730–737.
- Matsui, I., Matsui, E., Sakai, Y., Kikuchi, H., Kawarabayasi, Y., Ura, H., Kawaguchi, S., Kuramitsu, S., and Harata, K. 2000. The molecular structure of hyperthermostable aromatic aminotransferase with novel substrate specificity from *Pyrococcus horikoshii*. *J. Biol. Chem.* **275**: 4871–4879.
- McRee, D.E. 1999. XtalView/Xfit: A versatile program for manipulating atomic coordinates and electron density. *J. Struct. Biol.* **125**: 156–165.
- Merritt, E.A. and Murphy, M.E.P. 1994. Raster3D Version 2.0. A program for photorealistic molecular graphics. *Acta Crystallogr. Sect. D Biol. Crystallogr.* **50**: 869–873.
- Mizuguchi, H., Hayashi, H., Okada, K., Miyahara, I., Hirotsu, K., and Kagamiyama, H. 2001. Strain is more important than electrostatic interaction in controlling the pKa of the catalytic group in aspartate aminotransferase. *Biochemistry* **40**: 353–360.
- Moser, M., Müller, R., Battchikova, N., Koivulehto, M., Korpela, T., and Jansonius, J.N. 1996. Crystallization and preliminary X-ray analysis of phosphoserine aminotransferase from *Bacillus circulans subsp. alkalophilus*. *Protein Sci.* **5**: 1426–1428.
- Navaza, J. 1994. AMoRe: An automated package for molecular replacement. *Acta Crystallogr. A Fundam. Crystallogr.* **50**: 157–163.
- Neidhart, D.J. and Petsko, G.A. 1988. The refined crystal structure of subtilisin Carlsberg at 2.5 Å resolution. *Protein Eng.* **2**: 271–276.
- Noland, B.W., Newman, J.M., Hendle, J., Badger, J., Christopher, J.A., Tresser, J., Buchanan, M.D., Wright, T.A., Rutter, M.E., Sanderson, W.E., et al. 2002. Structural studies of *Salmonella typhimurium* ArnB (PmrH) aminotransferase: A 4-amino-4-deoxy-L-arabinose lipopolysaccharide-modifying enzyme. *Structure* **10**: 1569–1580.
- Otwinowski, Z. and Minor, W. 1997. Processing of X-ray diffraction data collected in oscillation mode. *Methods Enzymol.* **276**: 307–326.
- Schäfer, K., Magnusson, U., Scheffel, F., Schiefner, A., Sandgren, M.O., Diederichs, K., Welte, W., Hulsmann, A., Schneider, E., and Mowbray, S.L. 2004. X-ray structures of the maltose-maltodextrin-binding protein of the thermoacidophilic bacterium *Alicyclobacillus acidocaldarius* provide insight into acid stability of proteins. *J. Mol. Biol.* **335**: 261–274.
- Schneider, G., Kack, H., and Lindqvist, Y. 2000. The manifold of vitamin B6 dependent enzymes. *Struct. Fold. Des.* **8**: R1–R6.
- Sheldrick, G. and Schneider T. 1997. SHELXL: High-resolution refinement. *Methods Enzymol.* **277**: 319–343.
- Shirai, T., Suzuki, A., Yamane, T., Ashida, T., Kobayashi, T., Hitomi, J., and Ito, S. 1997. High-resolution crystal structure of M-protease: Phylogeny aided analysis of the high-alkaline adaptation mechanism. *Protein Eng.* **10**: 627–634.
- Shirai, T., Ishida, H., Noda, J., Yamane, T., Ozaki, K., Hakamada, Y., and Ito, S. 2001. Crystal structure of alkaline cellulase K: Insight into the alkaline adaptation of an industrial enzyme. *J. Mol. Biol.* **310**: 1079–1087.
- Snell, K. 1986. The duality of pathways for serine biosynthesis is a fallacy. *Trends Biochem. Sci.* **11**: 241–243.
- Sternier, R. and Liebl, W. 2001. Thermophilic adaptation of proteins. *Crit. Rev. Biochem. Mol. Biol.* **36**: 39–106.
- Ura, H., Nakai, T., Kawaguchi, S.I., Miyahara, I., Hirotsu, K., and Kuramitsu, S. 2001. Substrate recognition mechanism of thermophilic dual-substrate enzyme. *J. Biochem.* **130**: 89–98.
- Walsh, D.A. and Sallach, H.J. 1966. Comparative studies on the pathway for serine biosynthesis in animal tissues. *J. Biol. Chem.* **241**: 4068–4076.